Fabrication of Ge-ZnS multilayered optical filters for mid-infrared applications

Maxime Duris, Damien Deubel, Loïc Bodiou, Claude Vaudry, Jean-Claude Keromnes, Joël Charrier

Fabrication of Ge-ZnS multilayered optical filters for Mid-Infrared applications

M. Duris[1,2], D. Deubel[1,*], L.Bodiou[2], C. Vaudry[1], J.-C. Keromnes[1], and J. Charrier[2,*]

[1]KERDRY, 5 Rue Louis de Broglie, 22300 Lannion, France

[2]*Univ Rennes, CNRS, Institut FOTON - UMR 6082, F-22305 Lannion, France*

* Corresponding authors: Damien.Deubel@kerdry.com Joel.Charrier@univ-rennes1.fr

Highlights:

- Ion assisted electron beam deposition of Ge and ZnS single and multilayers
- Complex refractive indices of Ge and ZnS thin films extracted from FTIR spectra
- Design, deposition and simulation of mid-infrared filters made of up to 29 layers
- Demonstration of high and anti-reflection coatings in the long-wave infrared (LWIR)
- Dichroic filter with a low transmittance in MWIR and broadband bandpass in LWIR

Abstract:

Germanium/Zinc Sulphide (Ge/ZnS) single and multilayers are deposited by ion assisted electron beam deposition on Silicon substrates for applications in the 2-15 µm wavelength region. Refractive indices of Ge and ZnS thin films are extracted from measured reflectance and transmittance spectra. Several types of mid-infrared filters (high-, anti-reflection coatings and dichroic filters) with a number of layers ranging from 3 to 29 are then designed and deposited. The optical responses of fabricated mid-infrared filters show a good agreement between experimental spectra and simulation in the case of high- and anti-reflection coatings in the long-wave infrared but also for dichroic filters with a low transmittance in the mid-wave infrared and broadband bandpass in the long-wave infrared.

Keywords:

Broadband antireflection coating; Dichroic filter; Ion-assisted deposition; Electron beam evaporation; Germanium; Zinc Sulphide

1. Introduction

The mid-infrared (mid-IR), defined as the spectral region extending from 2 to 25 µm, covers the important atmospheric windows, 3-5 µm and 8-12 µm, and the molecular fingerprints of numerous gases, liquids and solids. Applications ranging from environmental monitoring and pollutant detection (discrimination of oil from water or ocean temperature, smoke and greenhouse gases detection, emerging water pollutant identification) to military and homeland security (trace explosives detection or target discrimination at night) through industrial and healthcare (food processing industry, methane detection around pipelines or pharmaceutical and medical products identification) can potentially benefit from discrete components operating in this wavelength window. In particular, several applications require the development of mid-IR filters (dichroic, broadband or bandpass filters). However, the implementation of these filters with enhanced material functionalities can only be achieved through the optimization of multi-layered coating based on mid-IR transparent materials.

Several materials with a transparency region extending far in the mid-IR have been associated to implement different kind of mid-IR filters. For example, narrow-bandpass filters in the long-wave infrared (LWIR) have been demonstrated using ZnSe/PbTe [1], low absorption ZnS/YF_3 and ZnS/ThF_4 antireflection coatings have been proposed to cover a large portion of the mid-IR µm range [2]-[4], Germanium substrates were also coated with the CdTe/CeF_3 + SrF_2 stack to obtain a low reflectance in the LWIR [5] or YbF_3 to demonstrate beam splitters [6] or broadband dispersive mirrors [7] operating, respectively, in the 4-8 µm and 6.5-11.5 µm spectral ranges. In the mid-wave infrared (MWIR), multilayered coatings incorporating oxide films (incorporating SiO or CeO_2 [8], HfO_2 [9] or Y_2O_3 [10]) can be used. The literature on mid-IR optical coatings therefore evidences that most stackings incorporates materials that are often qualified as toxic or even CMR (carcinogenic,

mutagenic or reprotoxic) hindering there potential application in regards with actual environment and health safety considerations and regulations.

For highly reflective coatings, reflectivity and bandwidth depend directly on the number of layers and on the refractive index contrast between the two materials constituting the stacking. For industrial applications, the selected materials must therefore not only be mid-IR transparent but also have a sufficiently large refractive index difference in order to avoid a prohibitive increase of layers number in the stacking. As adhesion difficulties are amplified in coatings with a large number of thick layers, mechanical properties of the films must also be taken into account.

As Germanium (Ge) and Zinc Sulfide (ZnS) thin layers exhibit high optical transmission of individual materials in the wavelength range of interest [11], good compatibility and a large refractive index contrast ($\Delta n \sim 2.0$), these materials are good candidates to implement mid-IR optical multilayered structures. A variety of techniques are used to prepare Ge and ZnS thin films. These include thermal evaporation [12], pulse laser deposition [13], [14], sputtering [15], [16], conventional electron beam evaporation [4], [9], [17]. Ion-assisted electron beam evaporation is particularly suited to the deposition of optical coatings and has therefore been gaining wide attention in an industrial context as it allows the production of a large number of high quality individual filters with high throughput [18]-[23].

In this paper, single films or multi-layers of Ge and ZnS were deposited by ion assisted electron-beam (e-beam) evaporation. The refractive indices of Germanium and zinc sulfide layers are first extracted from reflectance and transmittance spectra measured by Fourier Transform Infrared (FTIR) spectroscopy. Based on these measurements, various filters with a number of Ge and ZnS layers ranging from 3 to 29 are designed, manufactured and simulated. Finally, the fabrication of various filters on silicon substrates is illustrated in the case of high- and anti-reflection coatings in the long-wave infrared (LWIR) and also with a dichroic filters with a low transmittance in the mid-wave infrared (MWIR) and broadband bandpass in LWIR. Beside presenting results on complex mid-IR

optical filters made of Ge/Zns coatings comprising a few tens of layers deposited by ion-assisted electron-beam evaporation whose difficult production is evidenced by the very scarce literature on this specific subject [24], this paper demonstrates that the extensive knowledge of the refractive index of Ge and ZnS single layers can enable the engineering of any complex filter of up to ~30 layers on any substrate.

Specific applications often require the deposition on complex substrates in shape and/or composition such as chalcogenides fibers, Ge lenses or expensive III-V semiconductors substrate with limited availability. The optical filters described in this paper are all deposited on Si substrate and a versatile method of production and simulation of optical filters deposited on a cheap and standard Si substrate is presented. Indeed, this paper demonstrates that the good knowledge of Ge and ZnS optical constants (obtained from measurements and their extrapolation at longer wavelengths) and deposition parameters, enables the development of optical coatings that meet the target design specifications on a Si substrate. From the simulation of this stacking, with the extensive knowledge of the Si substrate properties, the optical response of the deposited multilayer can be extended on a semi-infinite substrate. From this step, the portability of the deposited stackings on any substrate can be inferred by numerical transposition of its optical response on a particular substrate provided its optical characteristics are available [25].

2. Experimental

Germanium and Zinc Sulphide thin films and multilayers were deposited on Silicon substrates (double-side polished, thickness=625 µm, resistivity=1-10 Ohm.cm) using a commercial BALZER 760 series thin film coater equipped with a 8-cm two gridded Kauffman ion source. Ge and ZnS sources were, respectively, composed of Ge powder (99.999%) and ZnS pellets or tablets (99.99%) and evaporated by a 10 kV electron beam gun. Prior deposition, Si substrates were cleaned with Decon90 by a standard procedure to remove surface contaminants, followed by ion beam pre-cleaning at 0.65

mA/cm^2 ion bombardment for 10 min. The deposition chamber was evacuated to a base pressure below 10^{-4} Pa (10^{-6} mbar) by a cryo-pump. During the ion-assisted deposition (IAD) process, argon pressure was maintained between 5×10^{-3} and 2×10^{-2} Pa (5×10^{-5} and 2×10^{-4} mbar). Single films of Ge and ZnS were deposited with a thickness of 2.5 µm for morphological, structural and optical characterizations. For the different fabricated filters, Ge or ZnS layers were alternatively deposited with thicknesses ranging from 90 to 1700 nm. As no optical monitoring apparatus was available to monitor the layer thickness during materials deposition, the deposition rate was controlled at 0.8 nm/s for Ge and 0.6 nm/s for ZnS by quartz-crystal oscillator with error of 0.1 nm/s and the substrate was heated to 150 and 170 °C during deposition.

Morphology of deposited films was analyzed using a profilometer (Veeco Dektak 150+ surface profiler) and a scanning electron microscope (SEM, Hitachi SU3500). Scanning electron images were recorded with a secondary electron Everhart-Thornley detector using an acceleration voltage of 15 kV and a working distance of 5 mm.

Transmittance and reflectance spectra were recorded using a Perkin Elmer Spectrum 100 Fourier-Transform Infra-Red (FTIR) spectrometer operating from 1.5 µm to 15µm with a resolution of 4 cm^{-1}. For reflectivity measurements, a calibrated 97.5% gold specular reflection standard served as reference between 1 and 25 µm. Recorded spectra were corrected from the absorption of the atmosphere (in particular the absorption lines of CO_2, water vapor and methane).

To assess the aging of the deposited coatings, peel tests with calibrated tape were performed to check adhesion after each deposition and 6 months later. Reflectance and transmittance spectra were also recorded several times in the 6 first months after deposition. All the optical filters presented thereafter have kept their mechanical properties as well as their spectral responses for at least 6 months.

Complex refractive indices of evaporated monolayers were extracted from recorded reflectance and transmittance spectra using a commercial software (The Essential Macleod v8.2, Thin

Film Center Inc., USA). With these data, the same software was used to perform a preliminary design of the multilayer stacking, in terms of number and thickness of the different layers, in order to obtain a specific filter response in reflection or transmission. After the evaporation procedure, the deposited mid-IR filters were also simulated with the same software to validate the optical constants and thicknesses previously measured.

3. Results and discussion

Scanning electron microscope (SEM) images were recorded for 2.5-µm thick Ge (Fig. 1a) and ZnS (Fig. 1b) thin films fabricated by ion assisted e-beam evaporation.

These images shows that the deposited Ge layers (Fig. 1a) are homogeneous whereas a dense columnar structure with low porosity is observed for ZnS layers (Fig. 1b). These morphologies are consistent with previous results obtained for low energy ion-assisted e-beam evaporation for Ge [26], [27] and ZnS [23], [28], [29]. Amorphous nature of the films and their homogeneity over the whole wafer area were confirmed by recording X-ray diffraction (not shown) and optical transmission/reflection spectra at different positions on the wafers. Furthermore, the morphology study of fabricated Ge and ZnS films by SEM shows the lack of cracks or defects which could compromise the quality of the interfaces between the different films in the multilayered structures. The root mean square roughness was measured by profilometry for the different evaporated films and reached ~85 nm for the 2.5-µm thick films.

Transmittance and reflectance experimental spectra were recorded between 1.5 and 9 µm. These spectra are displayed in Fig. 2 for 2.5 µm-thick Ge and ZnS layers.

Interference fringes are clearly visible on these figures and the fall of the curves above 8 µm is due to the absorption of O-H contaminant in Si substrate at 9 µm. Despite the care taken during

the experiment and the background correction, ripples are observed between 5.5 and 7.5 µm and are attributed to water absorption and absorption from dopants (un)intentionnaly incorporated in the Silicon substrate as they are already observed on transmittance and reflectance spectra recorded on bare 675-µm thick Czochralski Silicon substrate.

The optical constants (real and imaginary parts of the refractive index) of Germanium and Zinc Sulphide thin films were extracted from transmission and reflection spectra displayed in Fig. 2 by using the envelope method [30], [31]. In this technique, which assumes a homogeneous and isotropic film, two envelope curves are, respectively, defined based on the maxima and minima of a transmission curve and then a set of equations is applied to derive the thin film refractive index, extinction coefficient and thickness [32]. This method has been demonstrated to be also suitable to study inhomogenoeous and anisotropic thin films ([33]-[36]). The precision of the method [37] depends on the precision of the extrema positions $\lambda \pm \Delta\lambda$, their amplitudes and associated uncertainties expressed as $R\% \pm \Delta R\%$ and $T\% \pm \Delta T\%$ whereas $\Delta\lambda$ is related to the FTIR spectrometer resolution and is equal to 4 cm^{-1}. The transmittance and reflectance amplitude uncertainties ($\Delta T\%$ and $\Delta R\%$) were, respectively, found to be equal to 0.24 % and 0.32 % by taking into account metrological characteristics of the FTIR spectrometer and the repeatability over multiple reflectance and transmittance measurements on Si substrates, on samples consisting of single thin films deposited on a Si substrate and on multilayered coatings on Si substrate. The spectral dependence of real and imaginary parts of the Ge and ZnS refractive index obtained from these simulations are presented in Fig. 3.

From Fig. **3**, it can be observed that the optical constant variations of the two materials can be divided into two domains: a spectral region below 3 µm where Ge and ZnS are absorbent and dispersive and a second wavelength window above 3 µm where the refractive indices of both layers (Ge and ZnS) are constant which also corresponds to the spectral region where extinction coefficients are lower than 10^{-3} (Fig. **3**b). This feature is commonly observed for Ge thin films due to the

experimental conditions of ion-assisted e-beam evaporation [26]. In the non-absorbing region, deposited Zinc Sulfide thin films have a refractive index of 2.18 ± 0.04. This value is slightly lower than previously reported values of ZnS [38],[39] . Based on optical measurements in the visible spectrum, ion bombardment during deposition have been shown to improve the adhesion and hardness of the ZnS layer. Furthermore, ion-assisted deposition induces a loss of Sulfur mass in the ZnS single layers and multilayers which simultaneously results in a tensile mechanical strain and a reduction of the refractive index value [40].

The refractive index and extinction coefficient of Ge and ZnS were respectively adjusted (dashed lines in Fig. **3**) with Cauchy dispersions formula ($n = A + B/\lambda^2 + C/\lambda^4$, where n is refractive index, A, B and C are constants, λ is the wavelength) and an exponential model ($k(\lambda)=D \times \exp(E/\lambda)$ where D and E are constants). The results are summarized in Table 1 and Table 2.

In the wavelength range where both materials are considered transparent ($\lambda \geq 3.5$ µm), the refractive index contrast between both layers is slightly superior to 2 which enables fabrication of good performance filters with stacking composed of a reasonable numbers of layers. Multilayered structures were designed using Essential Macleod software based on the Ge and ZnS complex refractive indices using dispersion relations defined in Table 1 and Table 2. To engineer and simulate optical filters above 8-9 µm, where Si becomes absorbent, complex refractive indices values were extrapolated [41]-[44] from the Cauchy (refractive index) and exponential (extinction coefficient) adjustment parameters displayed in Table 1 and Table 2, respectively.

In a preliminary experiment to validate the measurement and adjustment of Ge and ZnS refractive indices and extinction coefficients, a mirror centered at 10.6 µm and a broadband antireflection coating with a central wavelength of 8 µm were designed and fabricated. The former filter is composed of 9 layers whereas the latter is made of 3 layers deposited on both sides of the Si wafer. The two multilayered filters are constituted by an alternative Ge and ZnS stacking (Fig. 4).

These images confirm the homogeneous nature and columnar structure of Ge and ZnS, respectively (Fig. 2). The strong contrast between successive layers of the stacking was used to obtain the layer thicknesses by performing image segmentation based on gray-level thresholding processing. The interfaces between individual layers as well as the surfaces of the multilayered structures were found to be smooth without any defect documenting applicability of ion-assisted e-beam evaporation for the fabrication of thin film stacks.

As for single films, optical characterizations of the optical filters (reflectance and transmittance spectra) were performed on at least three different locations over the 1.3 cm × 1.3 cm sample. These spectra showed good homogeneity of the materials deposition (in terms of optical constants and thickness of the different layers). The reflectance spectra of the high reflection filter measured with a FTIR spectrometer is presented in Fig. 5.

Fig. 5 shows that the fabricated mirror exhibits an optical reflectance spectrum in close correspondence with the target optical response. Indeed, for the mirror at 10.6 µm, the initial coating stacking was designed to obtain a reflection larger than 99 % at 10.6 µm. During deposition, the layer thicknesses slightly derived from designed quarterwave thicknesses which would have been equal to 635 nm and 1256 nm for Ge and ZnS materials, respectively. From SEM imaging (Fig. 4a), a variation of ~4% is obtained compared to quarterwave theoretical thickness for Ge layers, whereas it is ~2% for ZnS layers.

Simulation of experimental reflectance spectrum using the Essential MacLeod software is also displayed in Fig. 5. In this simulation, the dispersion of the Ge and ZnS refractive indices (Fig. 3) and the thickness of each layers extracted from Fig. 4a) are considered as fixed parameters for the simulation. The good agreement between experimental and simulated spectra suggests that the refractive indices extracted from single Ge and ZnS layers (Fig. 3) can be used to design any complex

mid-IR filter. The small discrepancies between spectra can be explained by taking into account the uncertainties on thicknesses measurement extracted from scanning electron microscopy images (this is especially noticeable for very thin films) and refractive indices inferred from FTIR measurements but also from small changes of the refractive index for films of different thicknesses. As an example, Fig. 5 depicts the effect of ±1% error assigned to Ge and ZnS layer thickness and refractive index on the filter optical response (dotted curves in Fig. 5). To derive these two curves, an important number of separate trials (128000) of reflectance simulations of the same stacking when ±1% error are arbitrarily assigned to Ge and ZnS layer thickness and refractive index were performed. From these reflectance spectra, a mean reflectance spectrum and a standard deviation were computed. The two dotted curved in Fig. 5 depict the effect of ±1% error assigned to Ge and ZnS layer thickness and refractive index and are obtained by, respectively, adding or subtracting, at each simulated wavelength, the standard deviation to the mean reflectance spectrum [17].

The transmittance spectrum of the 3-layer antireflection coating (Fig. 4b) that was designed to display a transmission larger than 90 % and a bandpass larger than 2 µm and centered at 8 µm is presented in Fig. 6. This coating was deposited on both sides of a Si wafer.

Again, a close correspondance between target design and fabricated filters is observed for this 3-layer antireflection filter. Fig. 6a also shows that the experimental spectrum can be simulated based on Ge and ZnS refractive indices dispersion (Fig. **3**), the different layer thicknesses inferred from Fig. **4**b and the transmission spectrum of the Si substrate recorded before the coating deposition. The similarity of these spectra indicates that deposition conditions are reproducible but also that optical characteristics of the Ge and ZnS films deposited in those conditions can be used to design various filters. In Fig. 6a, a dip in the transmission spectrum arising from the Si substrate absorption is observed around 9 µm. To remove the Si substrate contribution to the coating transmission and therefore to obtain the transmission spectrum of the coating itself, simulation were performed using the Essential MacLeod software. Indeed, taking into account the transmission of the

uncoated double-side polished Si substrate, a simulation of the transmission on a semi-infinite Si substrate can be computed. This extraction is presented in Fig. 6b and shows a simulation of the transmission that would be recorded on a semi-infinite Si substrate whose imaginary part of the refractive index is neglected. This spectrum has the advantage to enable the extrapolation of the Ge/ZnS multilayered coating transmission on any substrate.

Finally, to confirm Ge and ZnS complex refractive index values and further test the robustness of the deposition conditions, a 29-layer dichroic filter was designed to exhibit a low transmittance in the MWIR and broadband bandpass in LWIR (8-14 µm). The cross-section of the fabricated dichroic filter is displayed in Fig. 7.

Again, interfaces between individual Ge and ZnS layers are found to be smooth (inset of Fig. 7). The same method of gray-level thresholding was used to process these SEM images and extract the thickness of each layer. The transmittance spectrum of this dichroic filter deposited on 625-µm thick Si substrate is shown in Fig. 8a.

A good agreement is achieved between the experimental (solid line in Fig. 8a) and simulated (dashed line in Fig. 8a) transmittance spectra. The simulated spectra was once again calculated from thicknesses derived from SEM pictures (Fig. 7) and refractive indices of thin Ge and ZnS films (Fig. **3**). Although the dichroic filter fabrication was long and difficult to achieve considering the important number of layers and their very distinct thicknesses, the good correspondence between these spectra demonstrates that the deposition process and evaporation parameters are versatile and could serve as a basis for future on-demand filter design and fabrication. A sharp peak of transmission around 3 µm is observed in Fig. 8a but simulations show that it could be removed by increasing the number of layers.

Finally, to derive the coating transmission on a non-absorbing semi-infinite Si substrate, simulations were performed using the Essential Macleod software. The result of these computations is displayed in Fig. 8b from which it can be seen that this filter is consistent with the target design and exhibits a broadband bandpass above 8 µm and a low transmittance in the MWIR.

4. Conclusion

In conclusion, ion-assisted e-beam evaporation was used to deposit Ge and ZnS films and multilayer stackings. From the experimental recording of transmittance and reflectance spectra of 2.5-µm thick Ge and ZnS films, real and imaginary parts of the refractive index of these two materials were derived in the mid-IR wavelength range. An extinction coefficient lower than 10^{-3} was obtained for both materials above 3 µm. Different types of filters (high- and anti-reflection) were then designed for applications in the long-wave infrared and fabricated. A close correspondance between experimental and simulated reflectance and transmittance spectra was demonstrated. Complex dichroic coatings with up to 29 layers for applications in both MWIR and LWIR were subsequently fabricated and showed an optical response in good agreement with the target design. Therefore, these results confirm the industrial applicability of ion-assisted e-beam evaporation of Ge and ZnS films for the development of low-cost, high volume and versatile mid-IR complex filters.

Acknowledgments

M. D. acknowledges financial support from ANRT (Association Nationale Recherche Technologie) through a CIFRE grant N°2015/1042. Scanning Electron Microscopy imaging was performed in the CCLO-Renatech clean room facilities of Institut Foton. Equipment funding of Institut Foton was partly provided by the CPER Sophie.

References

[1] G. J. Hawkins, R. Hunneman, R. Sherwood, B.M. Barrett, Infrared filters and coatings for the High Resolution Dynamics Limb Sounder 6–18 µm, Appl. Opt, 39 (2000) 5221-5230. https://dx.doi.org/10.1364/AO.39.005221

[2] F. Lemarquis, G. Marchand, C. Amra, Design and manufacture of low-absorption ZnS–YF3 antireflection coatings in the 3.5–16-mm spectral range, Appl. Opt., 37 (1998) 4239-4244. https://dx.doi.org/10.1364/AO.37.004239

[3] A. V. Tikhonravov, V. G. Zhupanov, V. N. Fedoseev, and M. K. Trubetskov, Design and production of antireflection coating for the 8–10 µm spectral region, Opt. Express., 22 (2014) 32174-32179. https://dx.doi.org/10.1364/OE.22.032174

[4] A. Ghosh, A.S. Upadhyaya, Broad band antireflection coating on zinc sulphide simultaneously effective in SWIR, MWIR and LWIR regions, Infrared Phys. Technol., 52 (2009) 109-112. https://dx.doi.org/10.1016/j.infrared.2009.03.002

[5] I. Lubezky, E. Ceren, Z. Taubenfeld, H. Zipin, Efficient and durable AR coatings for Ge in the 8-11.5 µm band using synthesized refractive indices by evaporation of homogeneous mixtures, Appl. Opt., 22 (1983) 1828-1831 https://doi.org/10.1364/AO.22.001828.

[6] T. Amotchkina, M. Trubetskov, M. Schulz, and V. Pervak, Comparative study of NIR-MIR beamsplitters based on ZnS/YbF3 and Ge/YbF3, Opt. Express, 27 (2019) 5557-5569, https://doi.org/10.1364/OE.27.005557

[7] T. Amotchkina, M. Trubetskov, S. Ali Hussain, D. Hahner, D. Gerz, M. Huber, W. Schweinberger, I. Pupeza, F. Krausz, and V. Pervak, Broadband dispersive Ge/YbF3 mirrors for mid-infrared spectral range, Opt. Lett., 44 (2019), 5210-5213. https://doi.org/10.1364/OL.44.005210

[8] J. T. Cox, G. Hass, Antireflection Coatings for Germanium and Silicon in the Infrared, J. Opt. Soc. Am., 48 (1958) 677-680. https://dx.doi.org/10.1364/JOSA.48.000677.

[9] M. Bhatt, B.B. Nautiyal, P.K. Bandyopadhyay, High efficiency antireflection coating in MWIR region (3.6–4.9 µm) simultaneously effective for Germanium and Silicon optics, Infrared Phys. Technol., 53 (2010) 33-36. https://dx.doi.org/10.1016/j.infrared.2009.08.006

[10] R.Zarei Moghadam, H.Ahmadvand, M.Jannesari, Design and fabrication of multi-layers infrared antireflection coating consisting of ZnS and Ge on ZnS substrate, Infrared Phys. Technol. 75 (2016) 18–21. https://dx.doi.org/10.1016/j.infrared.2015.12.028

[11] H. Lin, Z. Luo, T. Gu, L. C. Kimerling, K. Wada, A. Agarwal, J. Hu, Mid-infrared integrated photonics on silicon: a perspective, Nanophotonics, 7 (2018) 393–420. https://dx.doi.org/10.1515/nanoph-2017-0085

[12] E. Barthélémy, S.Albert, C. Vigreux, A.Pradel, Effect of composition on the properties of Te-Ge thick films deposited by co-thermal evaporation, J.Non-Cryst.Solids. 356 (2010) 2175-2180. https://dx.doi.org/10.1016/j.jnoncrysol.2010.08.004.

[13] P. Schumacher, S. G. Mayr, and B. Rauschenbach, Topography evolution of germanium thin films synthesized by pulsed laser deposition, AIP Adv. 7 (2017) 045115. https://dx.doi.org/10.1063/1.4981800

[14] K.Hillie, C.Curren, H.Swart, ZnS thin films grown on Si(100) by XeCl pulsed laser ablation, Appl. Surf. Sci. 177 (2001) 73-77. https://dx.doi.org/10.1016/S0169-4332(01)00206-9

[15] D. J. Carney and R. Magnusson, Refractive index of sputtered germanium films in the 2.5-13 µm infrared spectral region, Opt. Mater. Express. 9 (2019) 3680-3690. https://dx.doi.org/10.1364/OME.9.003680

[16] F. Haque , K. S. Rahman , M. A. Islam , M. J. Rashid , M. Akhtaruzzaman , M. M. Alam , Z. A. Alathman , K. Sopian, N. Amin, 2014. Growth optimization of ZnS thin films by RF magnetron sputtering as prospective buffer layer in thin film solar cells. Chalcogenide Lett., 11 (2014) 189-197

[17] Y. Matsuoka, M. Semtsiv, S. Peters, and W. Ted Masselink, "Broadband multilayer antireflection coating for quantum cascade laser facets," Opt. Lett., 43 (2018) 4723-4726.

https://doi.org/10.1364/OL.43.004723
[18] T.D. Radjabov, I.E. Djamaletdinova, A.V. Sharudo, H. Hamidova, Ion-beam-assisted deposition as a method for production of effective optical coatings, Surf. Coat. Tech., 72 (1995) 99-102. https://dx.doi.org/10.1016/0257-8972(94)02335-2
[19] S.Scaglione, D.Flori, I.Soymié, A.Piegari, Laser optical coatings produced by ion beam assisted deposition, Thin Solid Films, 214 (1992) 188-193. https://ddx.doi.org/10.1016/0040-6090(92)90768-7
[20] S.Mohan, M.Ghanashyam Krishna, A review of ion beam assisted deposition of optical thin films, Vacuum, 46 (1995) 645-659. https://dx.doi.org/10.1016/0042-207X(95)00001-1
[21] J.R. McNeil, A.C. Barron, S.R. Wilson, and W.C. Herrmann, Ion-assisted deposition of optical thin films: low energy vs high energy bombardment, Appl. Opt., 23 (1984) 552-559. https://dx.doi.org/10.1364/AO.23.000552
[22] P.J. Martin, Ion-based methods for optical thin film Deposition, J. Mater. Sci, 21 (1986) 1–25. https://dx.doi.org/10.1007/BF01144693
[23] T.D. Radjabov, I.E. Djamaletdinova, A.V. Sharudo, H. Hamidova, Ion-beam-assisted deposition as a method for production of effective optical coatings, Surf. Coat. Tech., 72 (1995) 99-102. https://dx.doi.org/10.1016/0257-8972(94)02335-2
[24] F. Habel and V. Pervak, “Dispersive mirror for the mid-infrared spectral range of 9–11.5 μm”, Appl. Opt, 56, (2017) C71. https://doi.org/10.1364/AO.56.000C71
[25] J. Troles, L. Brilland, C. Caillaud, S. Venck, J.L. Adam, M. Duris, D. Deubel, L. Bodiou, J. Charrier, M. Carras, M. Brun, “Single-mode chalcogenide microstructured optical fibers: A solution for mid-IR fibered QCL”, SPIE Proceedings Volume 10899, Components and Packaging for Laser Systems V; 1089912 (2019), Event: SPIE LASE, 2019, San Francisco, California, United States. https://doi.org/10.1117/12.2506617
[26] Shih-Liang Ku, Cheng-Chung Lee, Jin-Sheng Tsai, Optical and structural properties of Ge films from ion-assisted deposition, Thin Solid Films. 517 (2008) 704-708. https://doi.org/10.1016/j.tsf.2008.08.112
[27] G. Pérez, A.M. Bernal-Oliva, E. Márquez, J.M. González-Leal, C. Morant, I. Génova, J.F. Trigo, J.M. Sanz, Optical and structural characterisation of single and multilayer germanium silicon monoxide systems. Thin Solid Films. 485 (2005) 274-283,1. https://doi.org/10.1016/j.tsf.2005.03.054
[28] Judith A. Ruffner, Marc D. Himel, Victor Mizrahi, George I. Stegeman, Ursula J. Gibson, Effects of low substrate temperature and ion assisted deposition on composition, optical properties, and stress of ZnS thin films, Appl. Opt., 28 (1989) 5209-52014. https://doi.org/10.1364/AO.28.005209
[29] H.K Pulker, E. Jung, Correlation between film structure and sorption behaviour of vapour deposited ZnS, cryolite and MgF2 films. Thin Solid Films. 9 (1972) 57-66. https://dx.doi.org/10.1016/0040-6090(72)90330-6
[30] R Swanepoel, Determination of the thickness and optical constants of amorphous silicon, J. Phys E: Sci. Instrum 16 (1983) 1214-1220. http://dx.doi.org/10.1088/0022-3735/16/12/023
[31] D.A.Minkov, Method for determining the optical constants of a thin film on a transparent substrate, J. Phys. D: Appl. Phys. 22 (1989) 199-205. http://dx.doi.org/10.1088/0022-3727/22/1/029
[32] M.M. Aslan, N.A. Webster, C.L. Byard, M.B. Pereira, C.M. Hayes, R.S. Wiederkehr, S.B. Mendes, Low-loss optical waveguides for the near ultra-violet and visible spectral regions with Al2O3 thin films from atomic layer deposition, Thin Solid Films 518 (2010) 4935–4940. https://dx.doi.org/10.1016/j.tsf.2010.03.011
[33] J. P. Borgogno, B. Lazarides, and E. Pelletier, "Automatic determination of the optical constants of inhomogeneous," Appl. Opt. 21, (1982) 4020-4029
[34] A. Edit Pap, K. Kordás, J. Vähäkangas, A. Uusimäki, S. Leppävuori, L. Pilon, S.Szatmári, Optical properties of porous silicon. Part III: Comparison of experimental and theoretical results, Opt. Mater., 28 (2006), 506-513.

[35] A. Popescu, D. Savastru, S. Miclos, Refractive index anisotropy in non-crystalline As_2S_3 films. Journal of Optoelectronics and Advanced Materials. 12 (2010) 1012-1018.
[36] S. Mendes, Envelope and waveguide methods: a comparative study of PbF_2 and CeO_2 birefringent films, Appl. Opt., 33 (1994) 2659-2663. http://dx.doi.org/10.1364/AO.33.002659
[37] J.C.Manifacier, J. Gasiot and J. P. Fillard, A simple method for the determination of the optical constants n,k and the thickness of weakly absorbing thin film, J. Phys E: Sci. Instrum. 9 (1976) 1002-1004. http://dx.doi.org/10.1088/0022-3735/9/11/032
[38] M. Debenham, Refractive indices of zinc sulfide in the 0.405–13-µm wavelength range, Appl. Opt., 23 (1984) 2238-2239. https://dx.doi.org/10.1364/AO.23.002238
[39] T. Amotchkina, M. Trubetskov, D. Hahner, and V Pervak, Characterization of e-beam evaporated Ge, YbF3, ZnS, and LaF3 thin films for laser-oriented coatings, Appl. Opt., 59 (2020) A40-A47 https://doi.org/10.1364/AO.59.000A40
[40] P.-F. Gu, Y. M. Chen, X. Q. Hu, J.-F. Tang, Properties of dielectric coatings produced by ion assisted deposition, Appl. Opt., 28 (1989) 3318-3322. https://doi.org/10.1364/AO.28.003318
[41] B. W. Morrissey and C. J. Powell, Interpolation of Refractive Index Data, Appl. Opt., 12, (1973) 1588-1591
[42] Y. Fang, D. Furniss, D. Jayasuriya, H. Parnell, Z.Q. Tang, D. Gibson, S. Bayya, J. Sanghera, A.B. Seddon and T.M. Benson, Methods for determining the refractive indices and thermo-optic coefficients of chalcogenide glasses at MIR wavelengths, Optical Materials: X, 2 (2019) 100030https://doi.org/10.1016/j.omx.2019.100030.
[43] Y. Jin, B. Song, C. Lin, P. Zhang, S. Dai, T. Xu, and Q. Nie, Extension of the Swanepoel method for obtaining the refractive index of chalcogenide thin films accurately at an arbitrary wavenumber, Opt. Express 25, (2017) 31273-31280
[44] D. Kushev, N. Zheleva, M.I. Gyulmezov, M.H Koparanova, An envelope method for determination of the optical constants of absorptive films on absorptive substrates, Infrared Physics. 34. (1993) 163–167, https://doi.org/10.1016/0020-0891(93)90005-R.

List of Tables:

Table 1. Cauchy adjustment parameters of Ge and ZnS refractive indices

Cauchy adjustment parameters	Ge	ZnS
A	4.1682	2.1741
B (μm^{-2})	0.4882	0.3501
C (μm^{-4})	0.9000	0.0001

Table 2. Exponential adjustment parameters of Ge and ZnS extinction coefficients

Exponential adjustment parameters	Ge	ZnS
D	0.00017	0.00014
E (μm)	6.5	4.2

Figure captions:

Fig. 1*:* Scanning electron microscope cross-sectional views of a) Germanium and b) Zinc Sulphide thin films.

Fig. 2: Transmittance and reflectance spectra of 2.5 μm-thick a), b) Germanium and c), d) Zinc sulphide thin films.

Fig. 3: a) refractive index and b) extinction coefficient of 2.5 μm-thick Ge and ZnS thin films as a function of wavelength

Fig. 4*:* Scanning electron microscope cross-sectional views of a) the high reflection filter at 10.6 μm and b) the antireflection filter with a band pass centered at 8 μm.

Fig. 5*:* Reflectance spectrum of the 9-layer filter, the solid and dashed curves correspond, respectively, to the experimental measurement and simulated spectrum based on experimental refractive indices and thicknesses derived from SEM imaging. Dotted curves depict a ±1% error effect (assign both to Ge and ZnS layer thickness and refractive index) on the simulated reflectance of the 9-layer filter.

Fig. 6: a) Experimental and simulated transmittance spectra of the 3-layer filter deposited on both sides of a 625 μm-thick Si substrate, b) Simulated spectra of the same 3-layer filter on a semi-infinite Si substrate.

Fig. 7: Scanning electron microscope cross-sectional view of a dichroic filter with a low transmittance in MWIR and broadband bandpass in LWIR. Inset shows a zoom-in view of the multilayered coating

Fig. 8: a) Experimental (solid curve) and simulated (dashed curve) transmittance spectra of the 29-layer dichroic filter on a 625-μm thick Si substrate, b) simulation transmission of the 29-layer dichroic filter on a semi-infinite Si substrate.

Figures:

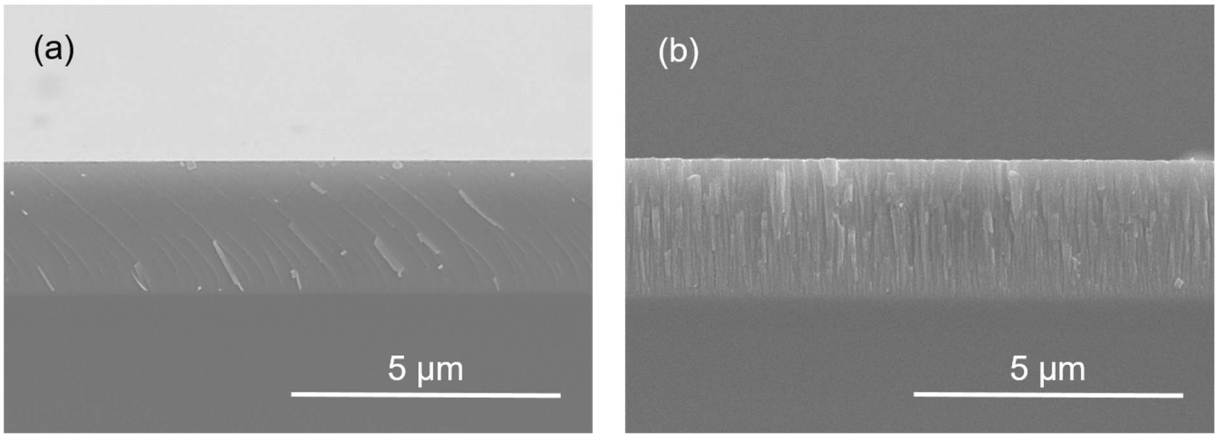

Fig. 1*:* Scanning electron microscope cross-sectional views of a) Germanium and b) Zinc Sulphide thin films.

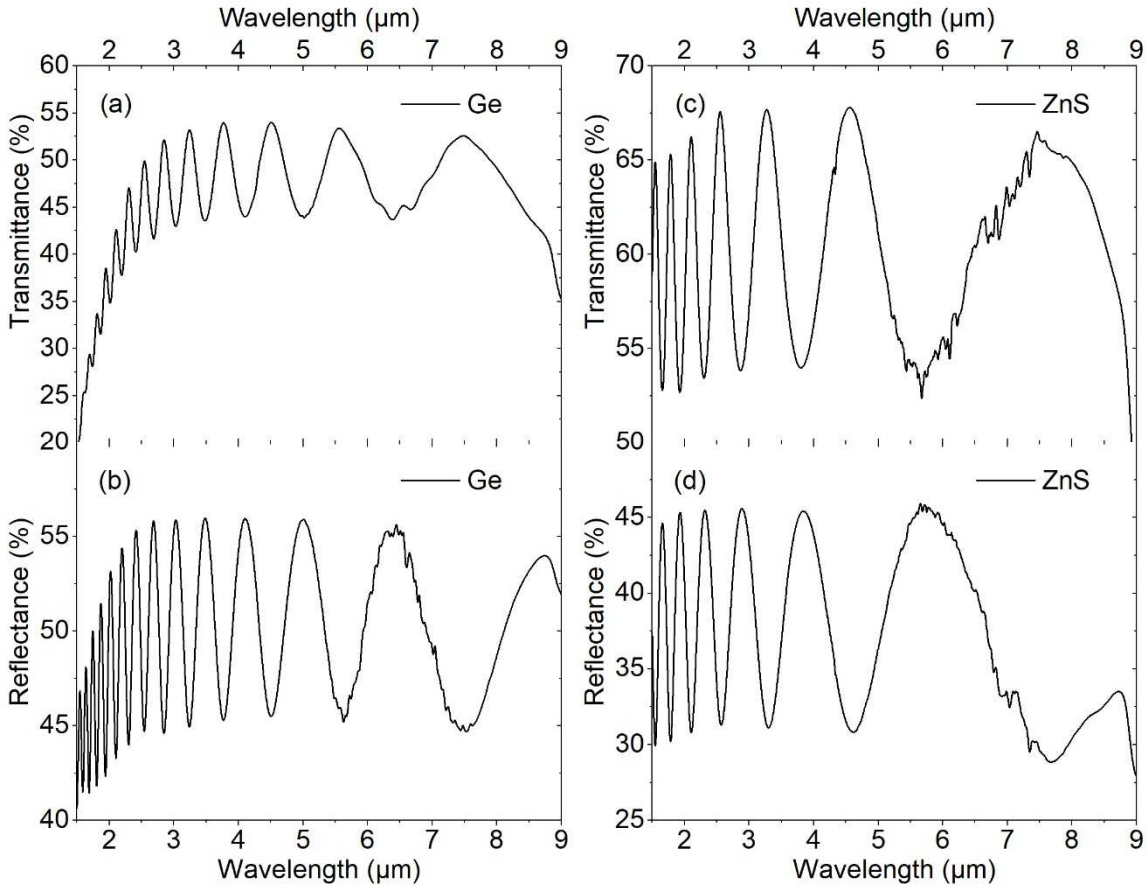

Fig. 2: Transmittance and reflectance spectra of 2.5 μm-thick a), b) Germanium and c), d) Zinc sulphide thin films.

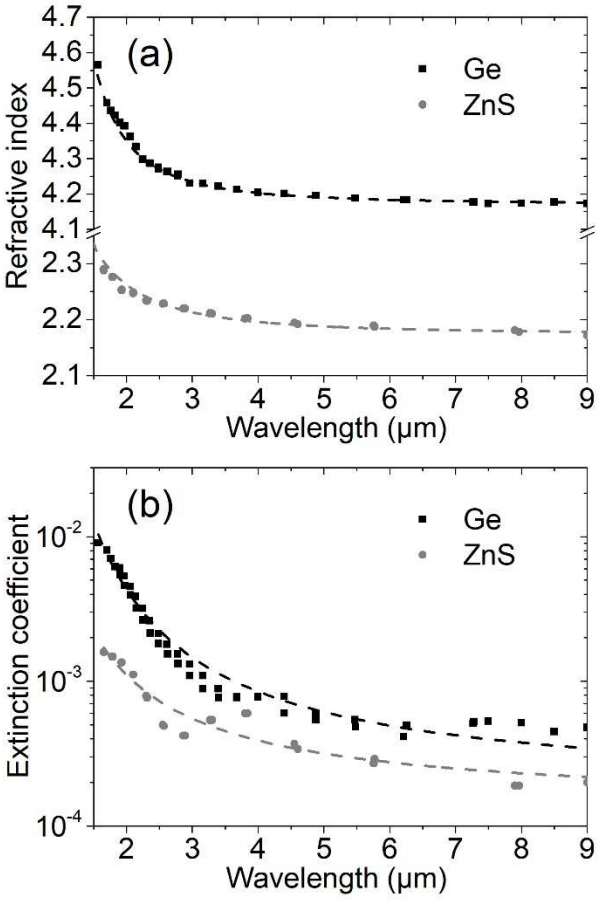

Fig. 3: a) refractive index and b) extinction coefficient of 2.5 μm-thick Ge and ZnS thin films as a function of wavelength

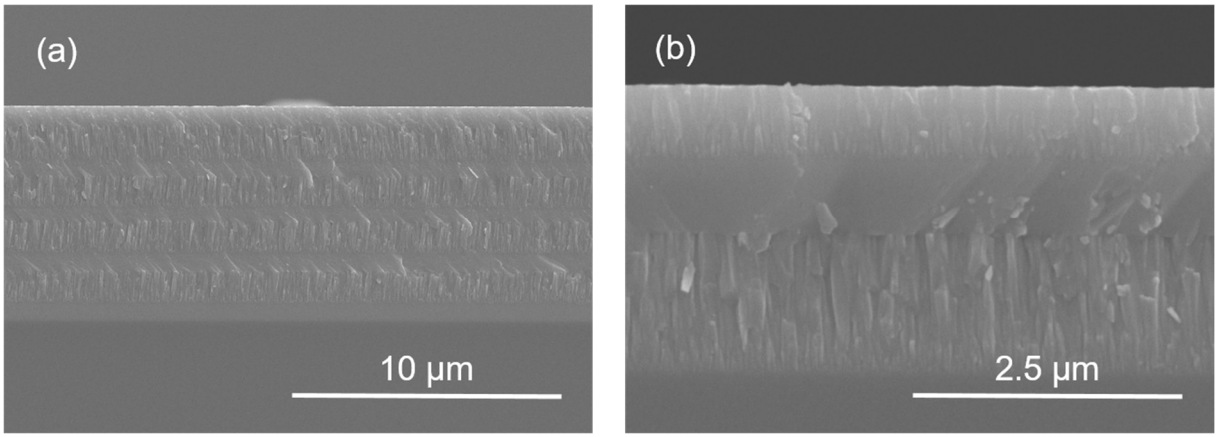

Fig. 4*:* Scanning electron microscope cross-sectional views of a) the high reflection filter at 10.6 µm and b) the antireflection filter with a band pass centered at 8 µm.

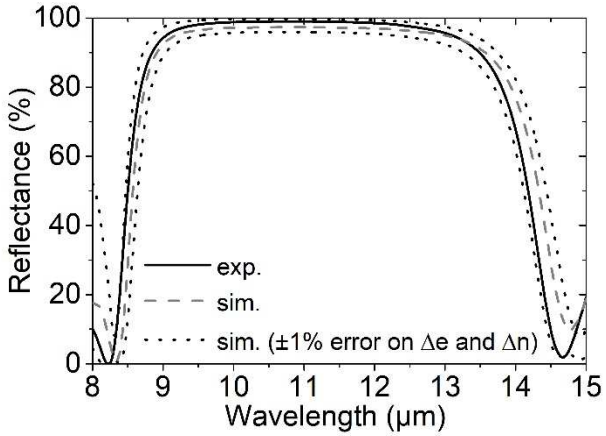

Fig. 5*:* Reflectance spectrum of the 9-layer filter, the solid and dashed curves correspond, respectively, to the experimental measurement and simulated spectrum based on experimental refractive indices and thicknesses derived from SEM imaging. Dotted curves depict a ±1% error effect (assign both to Ge and ZnS layer thickness and refractive index) on the simulated reflectance of the 9-layer filter.

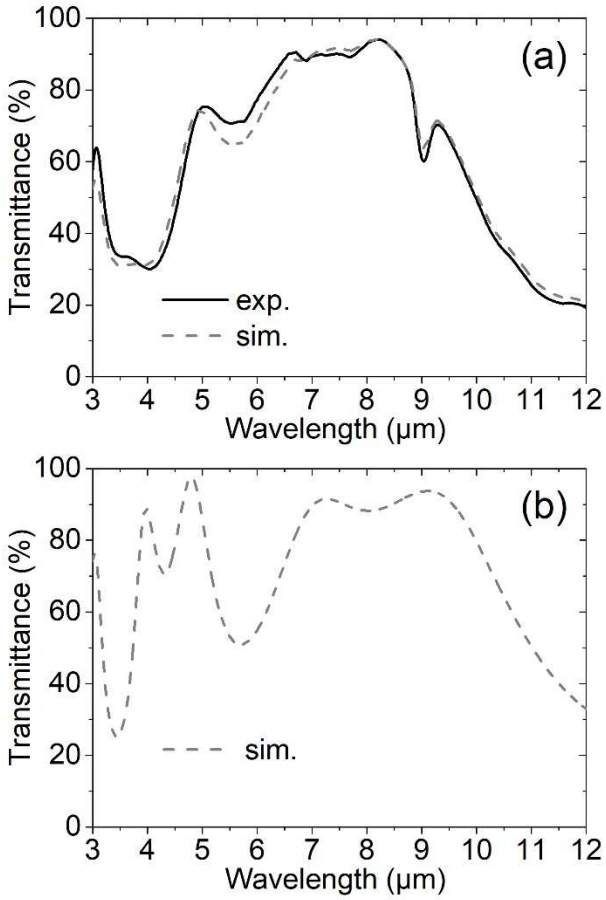

Fig. 6: a) Experimental and simulated transmittance spectra of the 3-layer filter deposited on both sides of a 625 μm-thick Si substrate, b) Simulated spectra of the same 3-layer filter on a semi-infinite Si substrate.

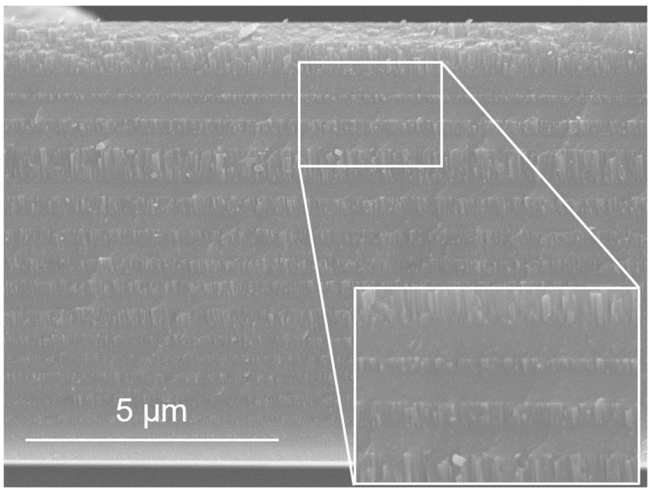

Fig. 7: Scanning electron microscope cross-sectional view of a dichroic filter with a low transmittance in MWIR and broadband bandpass in LWIR. Inset shows a zoom-in view of the multilayered coating

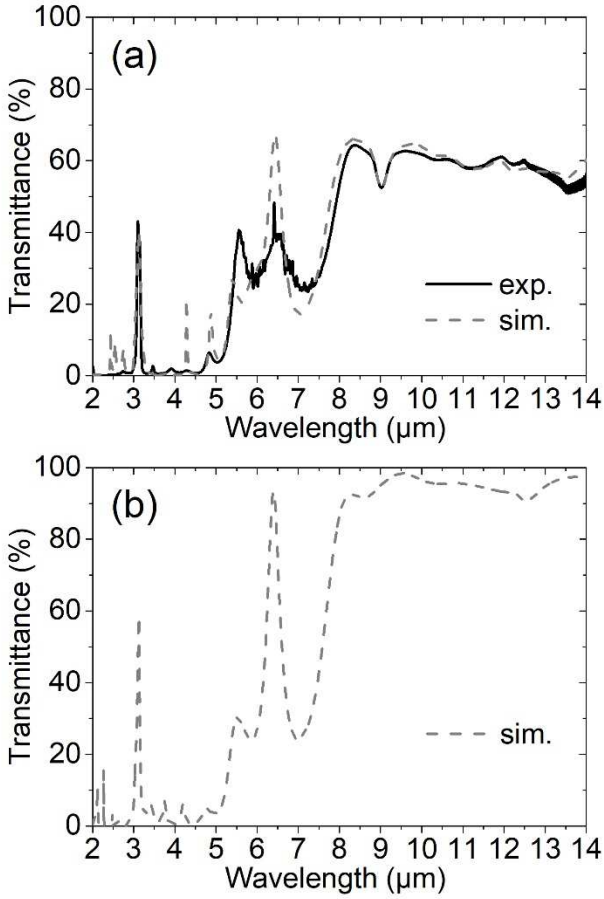

Fig. 8: a) Experimental (solid curve) and simulated (dashed curve) transmittance spectra of the 29-layer dichroic filter on a 625-μm thick Si substrate, b) simulation transmission of the 29-layer dichroic filter on a semi-infinite Si substrate.